THE JOURNAL OF PHYSICAL CHEMISTRY B

Article

pubs.acs.org/JPCB

Proton Transport under External Applied Voltage

Zhen Cao,[†] Revati Kumar,[‡] Yuxing Peng,[†] and Gregory A. Voth*,[†]

[†]Department of Chemistry, James Frank Institute, Computation Institute, The University of Chicago, 5735 South Ellis Avenue, Chicago, Illinois 60637, United States

[‡]Department of Chemistry, Louisiana State University, 736 Choppin Hall, Baton Rouge, Louisiana 70803, United States

ABSTRACT: Proton transport through an electrolyte layer between platinum electrodes under a range of applied voltages is explored using reactive molecular dynamics simulation. The proton transport process is decomposed into vehicular and Grotthuss hopping components, and the two mechanisms and their correlation are investigated as a function of applied voltage. At higher applied voltages, the effect of the hopping mechanism is much larger as compared with the vehicular mechanism. As the voltage is increased, the net correlation between the two mechanisms goes from negative to positive, and both the hopping frequency as well as the number of consecutive forward hops increases. This behavior results in a larger total diffusion constant at higher values of the voltage. The behavior of the hydrated excess proton is therefore substantially different under an applied external voltage than in the normal bulk water environment.

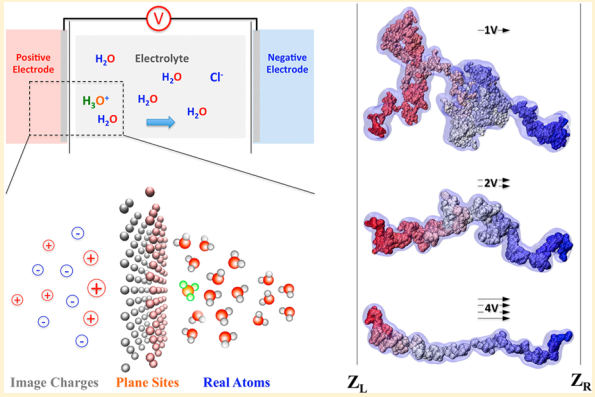

I. INTRODUCTION

Hydrated excess protons are the primary charge transport species in a number of systems ranging from energy storage to biological membranes.[1−4] In practice, this transport process often takes place under an electrostatic potential difference, and, in particular, in energy storage systems, the electrolyte is typically confined between electrodes with a voltage applied across the cell. Atomistic simulations can provide key insight, from both a dynamical as well as structural perspective,[5−16] into the charge transport processes in these systems. This, in turn, can be used to interpret experimental observations,[17−22] leading ultimately to the guided optimization of energy storage systems based on proton transport. However, comparatively few simulations have been carried out to study proton transport in electrochemical systems, and these concentrate on the electrochemical reduction of protons at the electrode surface[14,23,24] rather than the actual transport through the electrolyte. Moreover, recent work on the neat water platinum interface has revealed some interesting features including hindered dynamics and structuring of the water at these interfaces.[25,26] These dynamical effects are comparatively long-lived (tens of nanoseconds), and the structural correlations extend over large length scales (several nanometers). These studies suggest that simulations spanning long length and time scales will be necessary to study the proton transport mechanism near these types of metal/aqueous electrolyte interfaces. Computational investigations have been carried out to accurately model proton transport in the electrolyte region between electrodes in the presence and absence of an applied external voltage, resulting in fundamental insight into this complex charge transport process.

In addition to the usual vehicular diffusion, the proton can hop between water molecules, giving rise to the "Grotthuss shuttling" process.[27−29] This makes the modeling of proton transport particularly challenging because one needs a reactive description, lacking in conventional empirical force fields, involving both bond dissociation and formation. Ideally, one would like to employ ab initio molecular dynamics (MD) to study these types of systems, but the prohibitive computational cost precludes such studies in systems with time scales greater than the order of tens of picoseconds. Reactive MD models have been developed[28,30−32] to study proton transport in a wide range of systems, from biological ion channels,[32,33] to fuel cells.[34] The reactive methodology is based on a multiconfigurational approach, wherein the system is described as a linear combination of states, each with a different bonding topology, which is propagated in time allowing for smooth transitions from reactants to products. Previous studies have demonstrated that proton transport in aqueous media is particularly sensitive to the hydrogen bond environment.[35−37] Interestingly, the vehicular transport involves breaking of the neighboring hydrogen-bond network to let the hydronium transfer as a whole, while the Grotthuss mechanism requires a more complex process.[28,38−40]

Modeling proton transport in an aqueous electrolyte in the presence of an external voltage applied between the electrodes

Special Issue: James L. Skinner Festschrift

Received: January 31, 2014
Revised: April 9, 2014
Published: April 10, 2014

dx.doi.org/10.1021/jp501130m | J. Phys. Chem. B 2014, 118, 8090−8098

of an electrochemical cell adds another layer of complexity to the problem. An accurate description of the electrode−electrolyte interaction is necessary, which should include the polarization of typical metal electrodes by the electrolyte as well as the application of the applied voltage. Sprik and Siepmann[41] have developed a model of the electrode polarization, which, in turn, was extended to electrochemical systems by Madden and coworkers based on fluctuating charges on the electrode surface.[42,43] However, a computationally more efficient alternative, based on the method of images, developed previously by Petersen et al. that does not involve a computationally expensive iterative process is employed in this study.[44]

Recent studies have indicated that in electrochemical cells with interelectrode distances on the order of nanometers the charge transport ions are exposed to the large unscreened Coulomb fields of the electrodes, hence the term "Coulomb transport", giving rise to anomalously high currents.[44,45] These studies have focused on ions that exhibit traditional vehicular transport, unlike hydrated protons. However, given the importance of protons in electrochemical energy storage, the logical next step is to expand these studies to include hydrated protons as the charge transport species. Thus, a key goal of this work is to explore the proton transport mechanism in these types of cells with thin electrolyte layers in the presence and absence of an applied voltage.

The remaining sections of this article are organized as follows: The methodology to model the proton transport process in aqueous electrolytes between metal electrodes, under an external applied voltage, is introduced in Section II. In Section III, the details of the computations are outlined. The analysis of the structural and dynamical properties of the hydrated proton as a function of applied voltage is provided in Section IV. The contribution of the vehicular and the hopping mechanisms on the diffusion of the excess hydrated proton is investigated. The connection between the simulation results and the Coulomb transport phenomenon is also discussed. Section V presents concluding remarks.

II. METHODOLOGY

a. Multiconfigurational Reactive Model. As briefly mentioned in the Introduction, modeling proton transport in aqueous solutions is challenging because the hydrated proton charge defect can delocalize over several solvation shells, and the indistinguishable protons can shuttle between different water molecules, which leads to collective behavior.[28] A multiconfigurational MD framework, used previously to study proton transport in aqueous media,[28,30−32] is adopted here to model this Grotthuss shuttling of the delocalized proton. In spirit, this is similar to a quantum mechanical approach in that a Hamiltonian matrix is constructed. However, instead of treating the electronic degrees explicitly, this Hamiltonian is constructed in a basis of states that represent different bonding topologies (i.e., different classical hydronium ion configurations). The diagonal elements can be described by molecular mechanics force fields or even accurate electronic structure models.[46] For the sake of computational efficiency, a molecular-mechanics-based approach was used in this work. The off-diagonal elements represent the coupling between different bonding configurations that in turn allow for changes in the bonding topology. By construction, this is an eigenvalue problem, and the system is propagated on the adiabatic ground state obtained upon diagonalization of this Hamiltonian. The eigenvector, obtained on diagonalization, corresponding to the ground state is described by a set of coefficients $\{c_1, c_2, ..., c_N\}$, where N is the total number of states at a particular step in the simulation. The weight of any state i (i.e., a particular bonding topology) is given by the square of the corresponding coefficient, c_i^2. A detailed description of the multiconfigurational method can be found in refs 30−32. A suitable continuous coordinate is required to study the transport behavior of the delocalized excess proton. The center of excess charge (CEC) is used, defined as[2,31]

$$\vec{r}_{\mathrm{CEC}} = \sum_{i=1}^{N} c_i^2 \vec{r}_{\mathrm{COC}}^{\,i} \tag{1}$$

where $\vec{r}_{\mathrm{COC}}^{\,i}$ is the center of charge for the ith state, can represent the extent of the delocalization of the excess charge defect and can therefore be used to trace the movement of the hydrated excess proton.

b. Electrode−Electrolyte Model. A second challenging aspect of simulating electrochemical systems is an accurate representation of the electrode−electrolyte interaction and the application of a constant potential difference across the electrolyte. The delocalized hydrated proton is sensitive to the local environment,[28] and hence both the structural and dynamical properties are perturbed by the electric field originating from the polarization effect of the electrodes. To take this effect into account, a polarizable electrode model,[44] based on the method of images,[47] was incorporated into the multiconfigurational reactive MD framework. A brief description is as follows: Every real charge q_i of the electrolyte at a position z_i with respect to the positive electrode has two primary images of magnitude $-q_i$. These primary image charges induce higher order images on the electrode surface given by

$$q_{\mathrm{PE}} = \sum_i q_i z_i / D \tag{2a}$$

and

$$q_{\mathrm{NE}} = \sum_i q_i (1 - z_i/D) \tag{2b}$$

where the subscripts PE and NE represent the positive and negative electrode surfaces, respectively, and D is the distance between these surfaces. The application of an applied potential difference, V, across the cell is incorporated using a capacitor model, wherein an additional charge, which gives rise to this voltage, is applied on the electrode surface atoms. This additional charge on the electrode surface is given by $Q = VA\varepsilon_0/D$, where ε_0 is the vacuum permittivity and A is the area of electrode surface. The total charge on each electrode, in the presence of an applied voltage V, is now given by

$$q_{\mathrm{PE}} = \sum_i q_i z_i / D + Q \tag{3a}$$

and

$$q_{\mathrm{NE}} = \sum_i q_i (1 - z_i/D) - Q \tag{3b}$$

An outline of the algorithm used to calculate the energy due to the image charges is given later. As previously mentioned, each electrolyte charge q_i at a distance z_i from the positive electrode induces a primary image charge $-q_i$ on each electrode. This primary image on the positive (negative) electrode exerts an electrostatic force on every real electrolyte

dx.doi.org/10.1021/jp501130m | J. Phys. Chem. B 2014, 118, 8090−8098

charge that is equivalent to the electrostatic force exerted by a charge $-q_i$ at a distance $-z_i(2D - z_i)$ from the positive (negative) electrode. The electrostatic interaction energy due to the primary image is half the electrostatic energy between the primary image (at $-z_i$ or $2D - z_i$) and the electrolyte charges. The interaction of the higher order images on the electrode surface and the electrolyte is calculated in a different manner. Before starting the simulation, the electrolyte is removed from the cell setup. A unit test charge is distributed evenly over the atoms of each electrode surface. The force acting on another point test charge is simulated as a function of distance from the positive electrode and is tabulated. The force is integrated to give the potential energy, once again in a tabulated form. These data are stored, and during the simulation the higher order image–electrolyte charge interaction is obtained by multiplying the corresponding value from the table by the real electrolyte charge and the higher order electrode charge given by eqs 3a and 3b. For each diabatic state/bonding topology in the multiconfigurational model, the contribution of the electrode polarization to the energy is calculated very efficiently in this manner.

An accurate description of the electrode–electrolyte interaction includes not just the electrode polarization interaction, given by the method described in the previous paragraphs but also a representation of the interactions between the metal surface and the electrolyte. The three-body interaction model of Siepmann and Sprik was employed to describe this interaction between the water molecules and the platinum electrode atoms because it can distinguish different types of platinum surfaces as well as reproduce the structure of water adsorbed on different platinum clusters.[41] To determine the hydronium–platinum vdW interactions, we also carried out ab initio calculations on clusters consisting of platinum atoms and a single hydronium (see Figure 1) that are representative of

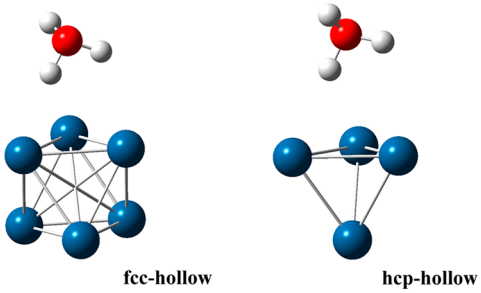

Figure 1. Two platinum–hydronium clusters used to parametrize the model. These are based on the clusters used to parametrize the platinum–water model.

typical platinum surfaces in electrochemical cells. Specifically, the fcc-hollow and hcp-hollow platinum clusters were constructed, and the hydronium was set above each platinum cluster. For each platinum configuration, the platinum surface–hydronium distance was scanned from 2.0 to 4.5 Å with an interval of 0.1 Å. The induced charges on the platinum atoms were obtained, using the fluctuating Gaussian charge model,[41] by solving the following set of equations

$$\frac{q_i}{\sqrt{\pi}\xi} + \sum_{\alpha}^{\text{per}} \frac{q_\alpha \operatorname{erf}(|r_i - r_\alpha|/\sqrt{2}\xi)}{|r_i - r_\alpha|} + \sum_{j\neq i}^{\text{ind}} \frac{q_j \operatorname{erf}(|r_i - r_j|/\xi)}{|r_i - r_j|} = V_0 \tag{4}$$

where ξ is the width of Gaussian distribution of charges, V_0 is the electrode voltage, q_i are the induced electrode charges, and q_α are the permanent charges. The electrostatic interactions between the hydronium and induced partial charges were subtracted from the ab initio energy for each cluster and the remainder was fit, using a least-squares method, to determine the remaining interaction components. This algorithm was used to determine the potential parameters for the water–platinum case, and hence, for consistency, the same method was employed for the hydronium–platinum case. The functional form of the vdW interaction used in this work consists of a two-body term and a three-body term, namely

$$U = U_{\text{2-body}} + U_{\text{3-body}} \tag{5}$$

where,

$$U_{\text{2-body}} = Ar_{ij}^{-\alpha} - Cr_{ij}^{-6} - Dr_{ij}^{-3} \exp\left[\frac{B}{(r - r_{\text{cut}})}\right] \exp\left[-8\left(\frac{\cos\varphi - 1}{4}\right)^4\right] \tag{6}$$

and

$$U_{\text{3-body}} = Er_{ij}^{-\beta} \exp\left(\frac{B}{r_{ij} - r_{\text{cut}}}\right) \exp\left[F \cos^2\left(\frac{\theta_{ijk}}{2}\right)\right] \tag{7}$$

The angle θ is between the oxygen–metal bond vector and the metal–metal bond vector, while φ is the angle between the oxygen–metal bond vector and the dipole moment vector of the hydronium (or water in the original paper by Siepmann and Sprik). The radial cut-off, r_{cut}, in the above equations is set to have a value of 3.2 Å. The first exponential term in both eqs 6 and 7 is set to zero if $r_{ij} \geq r_{\text{cut}}$. The three-body term captures the difference between the two surface structures, and it was left untouched during the fitting procedure and only the parameters A and C in the two-body term were fit. The values of the parameters for both the hydronium–platinum interaction (fit in this work) and water–platinum interaction (ref 41) are given in Table 1.

III. COMPUTATIONAL DETAILS

The Gaussian 09 suite of programs[48] was used to perform all ab initio electronic structure calculations. These were performed at the B3LYP level[49] of density functional theory with the LANL2DZ basis set[50] for the platinum atoms and 6-311g(d, p) basis set[51] for the hydronium atoms.

Reactive and nonreactive MD simulations were performed to gain insight into the proton transport mechanism under a range of applied voltages in the ultrathin electrolyte. The aqueous electrolyte solution consisted of 2591 water molecules and one extra hydronium and a neutralizing chloride anion. For the

Table 1. Values of the van der Waals Parameters (based on eqs 6 and 7) for the Water–Platinum and Hydronium–Platinum Interactions

species	A (kcal mol^{-1} Å^{11})	B (Å)	C (kcal mol^{-1} Å^6)	D (kcal mol^{-1} Å^3)	E (kcal mol^{-1} Å^{10})	F	α	β
H_2O	40 631	0.6	406.31	342.97	9.8	13.3	11	10
H_3O^+	149 176	0.6	1384.25	342.97	9.8	13.3	11	10

dx.doi.org/10.1021/jp501130m | J. Phys. Chem. B 2014, 118, 8090–8098

nonreactive simulations, the SPC/Fw water model[52] was used and the MS-EVB3 (Multistate Empirical Valence Bond Version 3) model, developed previously by Wu et al.,[30] was employed to carry out the reactive simulations that include the proton Grotthuss shuttling. In both cases, the chloride ion was modeled using the CHARMM force field,[53] and the Siepmann–Sprik model[41] was used for the water/hydronium–platinum vdW interactions. The electrolyte was confined between two platinum electrodes with the (111) surface facing the electrolyte. The reactive and nonreactive MD simulations were performed using a modified version of the LAMMPS[54] MD code. The electrolyte was pre-equilibrated in the constant NPT ensemble[55] to obtain the correct density. The platinum electrodes were then introduced perpendicular to the z direction at a distance of 57 Å apart, with the electrolyte between them. The (111) platinum surface of the electrode was exposed to the electrolyte. The x and y dimensions of the simulation box were 38.8 and 38.4 Å, respectively. A 3-D slab-like box was set up with the z-dimension nine times longer than the interelectrode distance, effectively resulting in a 2-D setup. The long-range interactions were calculated by using the particle–particle particle-mesh (PPPM) method[56] with the slab correction[57] added along the z direction. The simulations were performed under 0, 1, 2, and 4 V applied voltages, respectively, and data from 100 simulation trajectories with different initial configurations were accumulated to study the proton transport from the positive electrode to the negative electrode. For each simulation, the hydronium was constrained near the positive electrode, and the system was pre-equilibrated for over 100 ps before releasing the constraint. During the simulation, the coordinates of the whole system were recorded every 50 fs, and the reactive MD bonding topology states (including excess proton charge CEC coordinate) were recorded every 1 fs.

IV. RESULTS AND DISCUSSIONS

a. Hydronium–Platinum vdW Interaction. The ab initio energy of the hydronium–platinum clusters versus the model energy (red squares) is plotted in Figure 2. The small spread in the data along the straight black line with a slope of 1 and 0 y-intercept indicates the high quality of the fit. The root-mean-square deviation was found to be 0.24 kcal/mol. The values of the parameters for both the hydronium–platinum interaction (fit in this work) and water–platinum interaction (ref 41) are given in Table 1.

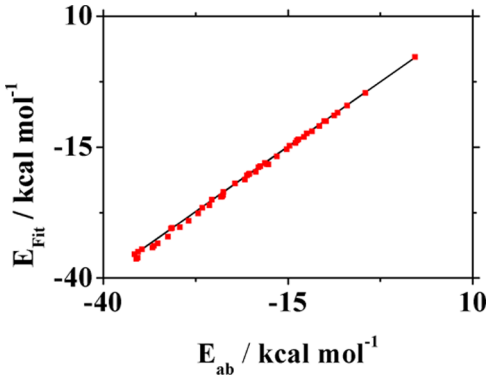

Figure 2. Plot of the ab initio energy (E_{ab}) of the clusters used to fit the hydronium–platinum interaction and the model energy (E_{fit}). The red circles show the actual values, and the black line with a slope of 1 and 0 y intercept is provided to indicate the small spread in the fit.

b. Influence of Applied Voltage on Structure. The electrostatic potential across the cell, $\Phi(z)$, where z is the distance from the positive electrode, was used to perform a meaningful decomposition of the electrolyte into different regions. Poisson's equation relates the electrostatic potential to the equilibrium charge density, $\rho(z)$

$$\nabla\Phi(z) = -\frac{\rho(z)}{\varepsilon_0} \tag{8}$$

The equilibrium charge density, as a function of z, was determined for each applied voltage, and the above equation was integrated to give the Poisson potential (plotted in Figure 3a). From the Figure, it is clear that the total Poisson potential drop across the cell for each case matches the applied voltage, which is a validation of our electrode model. The Poisson

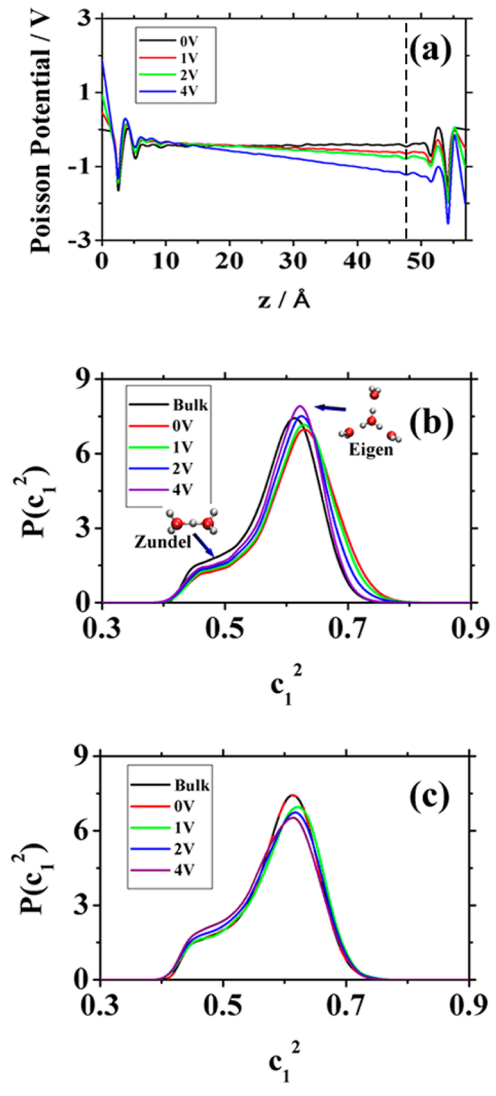

Figure 3. (a) Poisson potential drop for aqueous electrolyte. Depending on the fluctuation of the Poisson potential drop, the electrolyte is divided into the near-electrode region (relatively large fluctuations) extending to ~10 Å away from the electrode and the middle region (straight potential drop). (b,c) Probability distribution of the largest amplitude of the reactive MD bonding topology state for the negative near-electrode region and middle region, respectively. A value of $c_1^2 \approx 0.5$ corresponds to a Zundel-like $H_5O_2^+$ configuration, and a value of ~0.6 corresponds to an Eigen-like $H_9O_4^+$ configuration.

dx.doi.org/10.1021/jp501130m | J. Phys. Chem. B 2014, 118, 8090–8098

potential near the electrode surface shows large fluctuations, while the bulk-like middle region is relatively smooth. This allows for a separation of the electrolyte into distinct regions, namely, the near-electrode interfacial region with large fluctuations and a middle layer.

The delocalization of the hydrated proton positive charge defect in the different electrolyte layers was studied by plotting the distribution of the largest reactive MD state amplitude (c_1^2). A value of $c_1^2 = 1$ implies no delocalization of the excess proton, a pure classical hydronium cation, H_3O^+. A value of 0.5 corresponds to the excess proton being shared equally by two water molecules, the so-called Zundel species,[27] $H_5O_2^+$. A value of ~0.6 corresponds to an Eigen-like state,[27] wherein an excess proton is concentrated on the central water (central hydronium cation), but there is still some delocalization over the surrounding first solvation shell of three water molecules, that is, $H_9O_4^+$. Figure 3b,c shows the distribution of the largest probability amplitude of the reactive MD state near the negative electrode and the middle region, respectively.

Near the negative electrode, the water molecules form an ordered hydrogen bond network consisting of hexagonal rings, studied in detail by Chandler and coworkers,[25,26] rather than the usual disordered tetrahedral structures in liquid water. This results in more localization of the excess proton, indicated by the longer tail in the distribution of c_1^2 to larger values. To gain further insight into this behavior, the water structure near the ($-ve$) electrode surface was examined. Figure 4 shows the

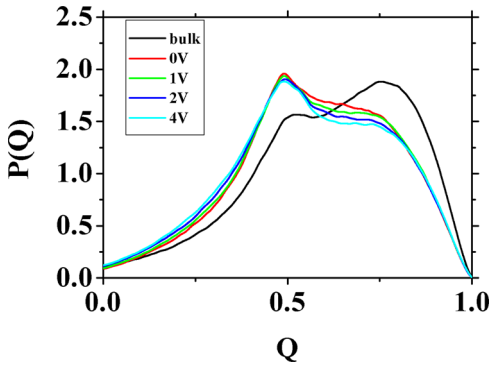

Figure 4. Distribution of the tetrahedral order parameter, Q, as a function of voltage for the water molecules in the negative near-electrode region. See the text for its definition. For comparison, the distribution in bulk water is also provided.

distribution of a tetrahedral order parameter, Q, in the near-($-ve$) electrode region as a function of applied voltage. Q is defined as[58,59]

$$Q = 1 - \frac{3}{8}\sum_{i=1}^{3}\sum_{j=i+1}^{4}\left[\cos(\Psi_{O_iO^*O_j}) + \frac{1}{3}\right]^2 \quad (9)$$

where $\Psi_{O_iO^*O_j}$ is the angle between two of the nearest four neighbors, i and j, and the central water (labeled *). A value of 1 indicates a perfect tetrahedral environment. For bulk water, there is a peak at 0.8, indicating that on average a large fraction of water molecules have an approximately tetrahedral solvation shell. In the case of water near the electrode surface (0 V case), a large fraction of water molecules form ring-like (typically six- and to some extent four-membered rings) structures,[25,26] which is clearly evident from the peak at ~0.5 and the diminishing of the peak at 0.8. As the voltage increases, the electric field near the electrode surface disrupts these highly constrained rings, leading to a decrease in the peak at 0.5 and a slight increase at smaller values of Q. This allows the excess proton charge defect to delocalize to a greater extent than at lower voltages. This is in keeping with the loss of the tail in c_1^2 to larger values and the slow increase in the Zundel species with increasing voltage. In the middle electrode region, there is no long tail in the distribution. The fraction of Zundel species increases with voltage and by 2 V is higher than the value in bulk aqueous solutions. The fraction of Eigen-like species decreases with applied voltage. The structural differences highlighted here are likely indicative of the environment, in which the proton transport occurs in many electrochemical systems.

c. Proton Diffusion: Vehicular Transport versus Grotthuss Hopping. To obtain a qualitative understanding of the excess proton diffusion, representative trajectories at three different voltages were examined. In Figure 5a–c, the 3-D

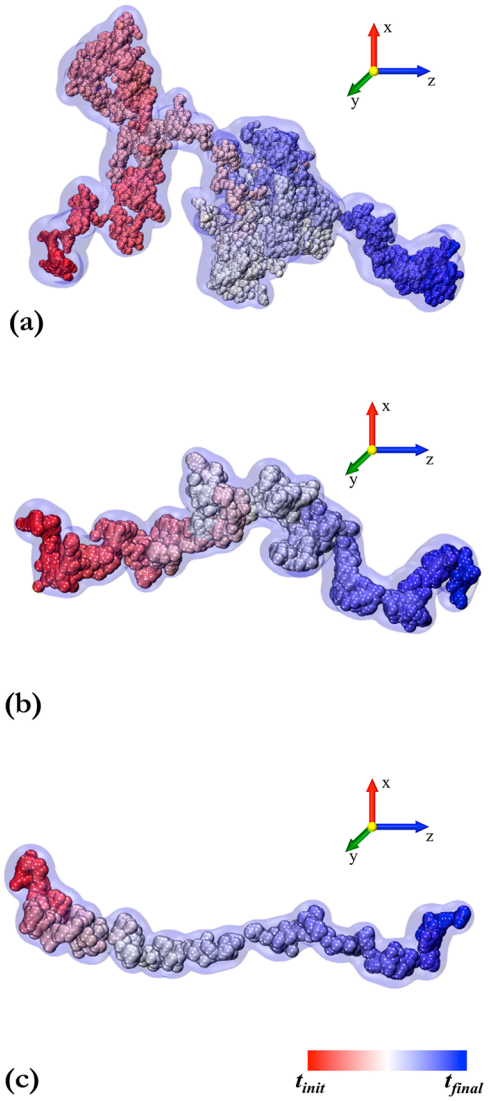

Figure 5. (a–c) Three representative trajectories for the 3-D diffusion of the excess proton charge defect center of excess charge (CEC) through the aqueous electrolyte under 1, 2, and 4 V applied voltages, respectively. The circles represent the position at time intervals of 100 fs. As the simulation progresses in time, the color changes gradually from red to blue.

dx.doi.org/10.1021/jp501130m | J. Phys. Chem. B 2014, 118, 8090–8098

diffusion of the CEC through the electrolyte under 1, 2, and 4 V applied voltages, respectively, is plotted. The circles represent the Cartesian positions of the excess proton CEC at 100 fs intervals. At the start, the circles are red in color, and as time progresses, the color changes gradually from red to blue. The z component represents the displacement along the direction perpendicular to the electrodes. On comparison of the three curves, it is clear that at lower voltages a larger number of circles are needed to traverse the same displacement in the z direction, indicating that the diffusion across the cell is slower at lower applied voltages, as is expected. In contrast, the diffusion is more unidirectional, with fewer back- and forth-type motions, at higher applied voltages.

The above behavior was quantitatively examined by calculating the diffusion coefficient for the CEC from its mean-squared displacement (MSD), and the results are shown in Figure 6. Consistent with Figure 5, the total diffusion

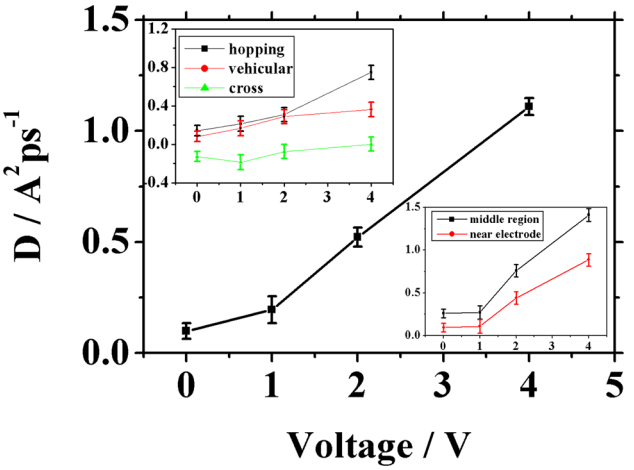

Figure 6. Plot of the total diffusion constants for the excess proton CEC as a function of applied voltage. The top inset shows the decomposition of the total diffusion into discrete (hopping), continuous (vehicular), and the cross product (correlated). The bottom inset shows the total diffusion in the middle electrolyte region and the near-negative electrode region.

coefficient increases with the increment of applied voltage. The bottom inset in Figure 6 shows the total diffusion constant in the middle electrolyte region and the near-negative electrode case as a function of voltage. Both curves are qualitatively similar to the total diffusion curve; however, the near-electrode case shows a consistently smaller value of diffusion constant, while the middle region shows a slightly larger value compared with the corresponding total diffusion constant. This is not surprising given that the water molecules in the near-electrode region form highly ordered and dynamically constrained configurations, thereby reducing both the vehicular and hopping diffusion.

To gain further insight into the transport mechanism, the total excess proton diffusion was decomposed into three components: diffusion due to hopping, vehicular diffusion, and a cross term.[60,61] This is determined by decomposing the total MSD itself into three terms, that is

$$\langle \vec{r}_{\mathrm{MSD}}^{\,2} \rangle = \langle \vec{r}_{\mathrm{d}}^{\,2} \rangle + \langle \vec{r}_{\mathrm{c}}^{\,2} \rangle + 2\langle \vec{r}_{\mathrm{d}} \cdot \vec{r}_{\mathrm{c}} \rangle \tag{10}$$

where $\vec{r}_{\mathrm{d}}$ represents the displacement from the hopping mechanism and $\vec{r}_{\mathrm{c}}$ represents the displacement from the vehicular mechanism. The definition used to distinguish the displacement from the two mechanisms is based on whether in a 100 fs time interval the proton hops, in which case, the displacement in this time interval contributes to the discrete/hopping MSD, whereas if no hopping takes place, it contributes to the continuous/vehicular case.[62] From these individual MSDs, the corresponding diffusion constant terms in eq 10 are obtained. The cross term is particularly intriguing because it gives a quantitative estimate of the correlation between the two transport mechanisms. The top inset in Figure 6 shows the results of the diffusion coefficients for each component. The zero voltage data are also shown in Figure 6 for comparison. The diffusion coefficient for the vehicular mechanism increases as the applied voltage is increased, which is consistent with the previous study of simple ions because they share a similar transport mechanism.[44] At higher voltages, the contribution of the hopping mechanism to the total charge transport becomes significantly greater than the vehicular component. This is in keeping with the structural data presented in the previous subsection, where with the increase in voltage the fraction of the Zundel species, necessary for proton hopping, increases.[28,29] Interestingly, the vehicular and hopping mechanisms are somewhat anticorrelated at low voltages, but at higher applied voltages, they are positively correlated. Hence, on increasing the applied voltage, both the vehicular and hopping diffusion increase, and at higher values of the applied voltage they reinforce each other, giving rise to a larger value of the total diffusion constant.

d. Analysis of Grotthuss Hopping. A quantitative estimate of the proton-hopping rate is determined by calculating a cumulative hopping function, $H(t)$, used in previous studies[63] of proton transport. It is defined as

$$H(t) = H(t - \Delta t) + H(\Delta t) \tag{11}$$

where, during the time interval Δt = 1 fs, $H(\Delta t)$ = 1 if the proton hops to the next water molecule, $H(\Delta t)$ = −1 if the proton hops back to the last water molecule, and $H(\Delta t)$ = 0 if no hop takes place. Figure 7a shows the hopping rate for three different trajectories, each at a different applied voltage. The curves show periods of fast jumps characterized by a steep rise as well as relatively flat resting periods. As the voltage increases, the value of the cumulative hopping count increases much faster in time, indicating a larger number of incidents of forward hopping and fewer resting stages. The slope of a linear fit to each curve gives an estimation of this effective forward hopping rate, and the value for 0 V is 41/ns, 1 V is 92/ns, 2 V is 112/ns, and for 4 V is 144/ns. For comparison, the value for bulk aqueous solution is ∼105/ns.

The curves also show oscillatory behavior due to the back-and-forth shuttling (or "rattling") of the proton between the regions of consecutive forward hops. To distinguish consecutive forward hopping of the excess charge from the back and forth rattling, we define a quantity called the concerted hopping number, n, which is a measure of the number of successive forward hops. The concerted hopping number can be determined by monitoring the changes in the hopping function. If in the time interval Δt the excess charge hops to a new water molecule, the hopping function for that interval is 1, that is, $H(\Delta t)$ = 1. If for n successive time intervals the value is 1, the concerted hopping number is n. For instance, if two consecutive hops take place with $H(\Delta t)$ = 1 followed by an event with $H(\Delta t)$ = −1, the concerted hopping number is two. Similarly, if n consecutive forward hopping events take place

dx.doi.org/10.1021/jp501130m | J. Phys. Chem. B 2014, 118, 8090−8098

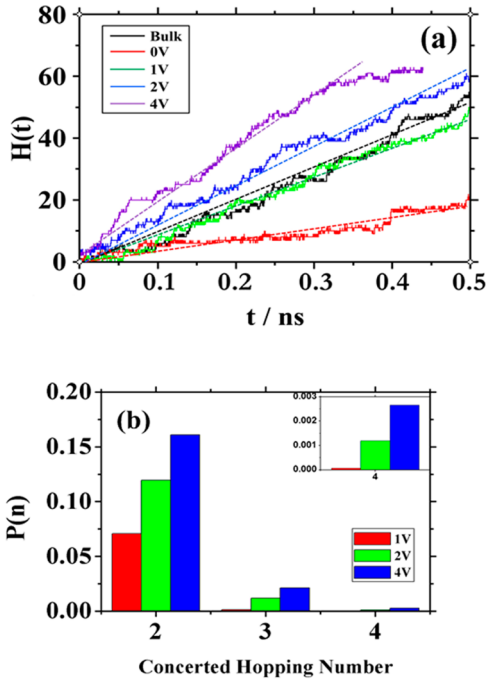

Figure 7. (a) Cumulative hopping function for three different voltages: bulk (black), 0 V (red), 1 V (green), 2 V (blue), and 4 V (purple). A linear fit to each curve is shown by the dotted line, and the slopes give an estimate of the forward hopping rate. (b) Probability distribution of the concerted proton hopping number for the three voltages: 1 (red), 2 (green), and 4 V (blue). The insert magnifies the case of four concerted hops.

with the n+1 step showing a backward hop, or no hop, the concerted hopping number is n. Figure 7b shows the distribution of the concerted hopping number as a function of applied voltage. As voltage increases, the probability of concerted hops (2, 3, and 4) increases. Two consecutive hops are the most typical type of concerted hopping seen at any voltage. A concerted hopping number of 4 is practically nonexistent at 1 V, while at 4 V there is a non-negligible fraction of 4, albeit at one tenth the probability seen for a value of 2 V. These results tie in well with not only the higher values of proton diffusion but also the positive correlation between vehicular and hopping diffusion seen at higher voltages.

e. Coulomb Transport Effect. The design of energy-storage devices with high energy and power density is the focus of intense research. A recently proposed route to achieving this is based on the development of devices with interelectrode separations on the order of nanometers. In typical energy storage devices, the charge carriers are screened from the effect of the surface electric field, and hence the charge transport is governed, to a large extent, by the bulk ion diffusion constant. However, in these ultrathin interelectrode devices, the transport of the charge carrier ions is influenced by the large electric fields on the electrode surface, which are no longer screened, giving rise to anomalously high currents, the so-called "Coulomb transport" effect.

To verify Coulomb transport, the effective current as a function of applied voltage was calculated in the ultrathin electrolytes simulated in this work. The simulations carried out in this work did not involve charge transfer (redox) reactions that are a necessary component of electrochemical cells; however, one can still evaluate the effective current because it is directly related to the mobility of the charge carriers in the electrolyte, provided the reaction overpotential due to the redox reaction does not dominate over the Ohmic resistance in the bulk electrolyte. Hence, the ratio of the diffusion constant in these simulations to the value in bulk aqueous solutions essentially gives an estimate of the ratio between the effective current and the limiting current due to bulk diffusion. This ratio of the effective current to the current due to the bulk diffusion limit, as a function of applied voltage, is shown in Figure 8 for

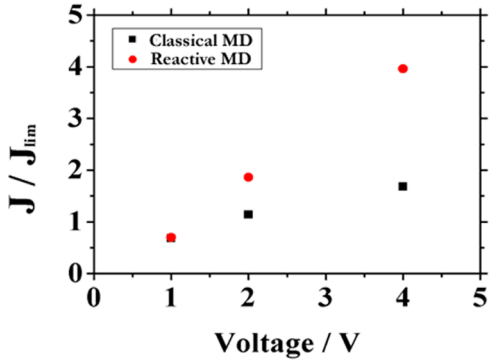

Figure 8. Linear relationship between the current density and the applied voltage. The squares and the circles represent the ratio of the effective current to the current due to the bulk diffusion limit for both the reactive (Grotthuss shuttling) and classical hydronium (no shuttling) MD simulations, respectively.

both the reactive Grotthuss shuttling and nonreactive proton transport simulations. In typical devices with interelectrode distances on the order of micrometers or higher this ratio starts to plateau around 2 to 3 V,[45,64] but here there is an increase in the current beyond the usual plateauing effect, an indication of Coulomb transport. At higher voltages, the current due to the reactive MD model is greater than the nonreactive case, and by 4 V the difference is pronounced, with the reactive value more than twice that of the nonreactive case. This highlights the importance of incorporating the proton-hopping process in any realistic simulation of these types of energy-storage devices.

V. CONCLUDING REMARKS

A reactive MD framework has been developed to accurately model proton transport in a prototypical energy storage system that consists of an aqueous electrolyte held between metal electrodes with an applied external voltage. This method incorporates the multiconfigurational MD approach to model proton transport including Grotthuss shuttling as well as an accurate, physically motivated representation of the electrode–electrolyte interaction. The results indicate that with increase in applied voltage the proton diffusion increases monotonically but in a nonlinear fashion and the overall behavior of the hydrated proton becomes quite different from the bulk water case. The proton diffusion mechanism still consists of two processes: a vehicular motion as well as Grotthuss proton hopping. At low applied voltages, these two processes are somewhat anticorrelated, whereas at higher voltages a net positive correlation contributes to the higher values of the coefficient of self-diffusion. Moreover, there is a marked increase in concerted proton hops, which contributes to a nonlinear increase in the excess proton diffusion rate with the increase in applied voltage. On examining the current due to proton diffusion, the ratio of the effective current to the current due to bulk diffusion was found to increase linearly with

dx.doi.org/10.1021/jp501130m | J. Phys. Chem. B 2014, 118, 8090–8098

voltage, with the increase being much larger for the reactive simulations compared with the nonreactive case of a "classical" nonhopping hydronium cation. This result is consistent with the proposed Coulomb transport process, in which charge-carrier transport is determined by the strong electric fields from the electrode surface charges in ultrathin interelectrode spacings.

AUTHOR INFORMATION

Corresponding Author

*E-mail: gavoth@uchicago.edu.

Notes

The authors declare no competing financial interest.

ACKNOWLEDGMENTS

This research was partially supported by the Office of Naval Research (ONR Grant N0014-12-1-1021) and the National Science Foundation (NSF grant CHE-1214087). This work was partially completed with resources provided by the University of Chicago Research Computing Center (RCC). We thank Prof. Henry White and Dr. Christopher Knight for valuable discussions.

REFERENCES

(1) Marx, D.; Chandra, A.; Tuckerman, M. E. Aqueous Basic Solutions: Hydroxide Solvation, Structural Diffusion, and Comparison to the Hydrated Proton. *Chem. Rev.* **2010**, *110*, 2174−2216.

(2) Voth, G. A. Computer Simulation of Proton Solvation and Transport in Aqueous and Biomolecular Systems. *Acc. Chem. Res.* **2006**, *39*, 143−150.

(3) Weinberg, D. R.; Gagliardi, C. J.; Hull, J. F.; Murphy, C. F.; Kent, C. A.; Westlake, B. C.; Paul, A.; Ess, D. H.; McCafferty, D. G.; Meyer, T. J. Proton-Coupled Electron Transfer. *Chem. Rev.* **2012**, *112*, 4016−4093.

(4) Wraight, C. A. Chance and design—Proton transfer in water, channels and bioenergetic proteins. *Biochim. Biophys. Acta* **2006**, *1757*, 886−912.

(5) Bonthuis, D. J.; Gekle, S.; Netz, R. R. Dielectric Profile of Interfacial Water and its Effect on Double-Layer Capacitance. *Phys. Rev. Lett.* **2011**, *107*, 166102.

(6) Duan, S.; Xu, X.; Tian, Z. Q.; Luo, Y. Hybrid molecular dynamics and first-principles study on the work function of a Pt(111) electrode immersed in aqueous solution at room temperature. *Phys. Rev. B* **2012**, *86*, 045450.

(7) Ikeshoji, T.; Otani, M.; Hamada, I.; Okamoto, Y. Reversible redox reaction and water configuration on a positively charged platinum surface: first principles molecular dynamics simulation. *Phys. Chem. Chem. Phys.* **2011**, *13*, 20223−20227.

(8) Letchworth-Weaver, K.; Arias, T. A. Joint density functional theory of the electrode-electrolyte interface: Application to fixed electrode potentials, interfacial capacitances, and potentials of zero charge. *Phys. Rev. B* **2012**, *86*, 075140.

(9) Otani, M.; Hamada, I.; Sugino, O.; Morikawa, Y.; Okamoto, Y.; Ikeshoji, T. Structure of the water/platinum interface - a first principles simulation under bias potential. *Phys. Chem. Chem. Phys.* **2008**, *10*, 3609−3612.

(10) Song, F. H.; Li, B. Q.; Liu, C. Molecular Dynamics Simulation of Nanosized Water Droplet Spreading in an Electric Field. *Langmuir* **2013**, *29*, 4266−4274.

(11) Spohr, E. Computer simulation of the structure of the electrochemical double layer. *J. Electroanal. Chem.* **1998**, *450*, 327−334.

(12) Spohr, E. Molecular dynamics simulations of water and ion dynamics in the electrochemical double layer. *Solid State Ionics* **2002**, *150*, 1−12.

(13) Torii, D.; Ohara, T. Molecular dynamics study on ultrathin liquid water film sheared between platinum solid walls: Liquid structure and energy and momentum transfer. *J. Chem. Phys.* **2007**, *126*, 154706.

(14) Wilhelm, F.; Schmickler, W.; Spohr, E. Proton transfer to charged platinum electrodes. A molecular dynamics trajectory study. *J. Phys.: Condens. Matter* **2010**, *22*, 175001.

(15) Winter, B.; Faubel, M.; Hertel, I. V.; Pettenkofer, C.; Bradforth, S. E.; Jagoda-Cwiklik, B.; Cwiklik, L.; Jungwirth, P. Electron Binding Energies of Hydrated H3O+ and OH-: Photoelectron Spectroscopy of Aqueous Acid and Base Solutions Combined with Electronic Structure Calculations. *J. Am. Chem. Soc.* **2006**, *128*, 3864−3865.

(16) Xia, X.; Berkowitz, M. L. Electric-Field Induced Restructuring of Water at a Platinum-Water Interface: A Molecular Dynamics Computer Simulation. *Phys. Rev. Lett.* **1995**, *74*, 3193−3196.

(17) Carrasco, J.; Hodgson, A.; Michaelides, A. A molecular perspective of water at metal interfaces. *Nat. Mater.* **2012**, *11*, 667−674.

(18) Hsieh, C.; Campen, R. K.; Okuno, M.; Backus, E. H. G.; Nagata, Y.; Bonn, M. Mechanism of vibrational energy dissipation of free OH groups at the air−water interface. *Proc. Natl. Acad. Sci. U.S.A.* **2013**, *110*, 18780−18785.

(19) Kuna, J. J.; Voitchovsky, K.; Singh, C.; Jiang, H.; Mwenifumbo, S.; Ghorai, P. K.; Stevens, M. M.; Glotzer, S. C.; Stellacci, F. The effect of nanometre-scale structure on interfacial energy. *Nat. Mater.* **2009**, *8*, 837−842.

(20) Ni, Y.; Gruenbaum, S. M.; Skinner, J. L. Slow hydrogen-bond switching dynamics at the water surface revealed by theoretical two-dimensional sum-frequency spectroscopy. *Proc. Natl. Acad. Sci. U.S.A.* **2013**, *110*, 1992−1998.

(21) Nie, S.; Feibelman, P. J.; Bartelt, N. C.; Thurmer, K. Pentagons and Heptagons in the First Water Layer on Pt(111). *Phys. Rev. Lett.* **2010**, *105*, 026102.

(22) Thürmer, K.; Bartelt, N. C. Nucleation-Limited Dewetting of Ice Films on Pt(111). *Phys. Rev. Lett.* **2008**, *100*, 186101.

(23) Schmickler, W.; Wilhelm, F.; Spohr, E. Probing the temperature dependence of proton transfer to charged platinum electrodes by reactive molecular dynamics trajectory studies. *Electrochim. Acta* **2013**, *101*, 341−346.

(24) Wilhelm, F.; Schmickler, W.; Nazmutdinov, R. R.; Spohr, E. A model for proton transfer to metal electrodes. *J. Phys. Chem. C* **2008**, *112*, 10814−10826.

(25) Limmer, D. T.; Willard, A. P.; Madden, P.; Chandler, D. Hydration of metal surfaces can be dynamically heterogeneous and hydrophobic. *Proc. Natl. Acad. Sci. U.S.A.* **2013**, *110*, 4200−4205.

(26) Willard, A. P.; Limmer, D. T.; Madden, P. A.; Chandler, D. Characterizing heterogeneous dynamics at hydrated electrode surfaces. *J. Chem. Phys.* **2013**, *138*, 184702.

(27) Agmon, N. The Grotthuss mechanism. *Chem. Phys. Lett.* **1995**, *244*, 456−462.

(28) Knight, C.; Voth, G. A. The Curious Case of the Hydrated Proton. *Acc. Chem. Res.* **2012**, *45*, 101−109.

(29) Markovitch, O.; Chen, H.; Izvekov, S.; Paesani, F.; Voth, G. A.; Agmon, N. Special Pair Dance and Partner Selection: Elementary Steps in Proton Transport in Liquid Water. *J. Phys. Chem. B* **2008**, *112*, 9456−9466.

(30) Wu, Y.; Chen, H.; Wang, F.; Paesani, F.; Voth, G. A. An Improved Multistate Empirical Valence Bond Model for Aqueous Proton Solvation and Transport. *J. Phys. Chem. B* **2008**, *112*, 467−482.

(31) Day, T. J. F.; Soudackov, A. V.; Euma, M.; Schmitt, U. W.; Voth, G. A. A second generation multistate empirical valence bond model for proton transport in aqueous systems. *J. Chem. Phys.* **2002**, *117*, 5839−5849.

(32) Swanson, J. M.; Maupin, C. M.; Chen, H.; Petersen, M. K.; Xu, J.; Wu, Y.; Voth, G. A. Proton Solvation and Transport in Aqueous and Biomolecular Systems: Insights from Computer Simulations. *J. Phys. Chem. B* **2007**, *111*, 4300−4314.

(33) Peng, Y.; Voth, G. A. Expanding the view of proton pumping in cytochrome c oxidase through computer simulation. *Biochim. Biophys. Acta* **2012**, *1817*, 518−525.
(34) Jorn, R.; Savage, J.; Voth, G. A. Proton Conduction in Exchange Membranes across Multiple Length Scales. *Acc. Chem. Res.* **2012**, *45*, 2002−2010.
(35) Day, T. J. F.; Schmitt, U. W.; Voth, G. A. The Mechanism of Hydrated Proton Transport in Water. *J. Am. Chem. Soc.* **2000**, *122*, 12027−12028.
(36) Feng, S.; Savage, J.; Voth, G. A. Effects of Polymer Morphology on Proton Solvation and Transport in Proton-Exchange Membranes. *J. Phys. Chem. C* **2012**, *116*, 19104−19116.
(37) Cao, Z.; Peng, Y.; Yan, T.; Li, S.; Li, A.; Voth, G. A. Mechanism of Fast Proton Transport along One-Dimensional Water Chains Confined in Carbon Nanotubes. *J. Am. Chem. Soc.* **2010**, *132*, 11395−11397.
(38) Lapid, H.; Agmon, N.; Petersen, M. K.; Voth, G. A. A bond-order analysis of the mechanism for hydrated proton mobility in liquid water. *J. Chem. Phys.* **2005**, *122*, 014506.
(39) Berkelbach, T. C.; Lee, H.; Tuckerman, M. E. Concerted Hydrogen-Bond Dynamics in the Transport Mechanism of the Hydrated Proton: A First-Principles Molecular Dynamics Study. *Phys. Rev. Lett.* **2009**, *103*, 238302.
(40) Tuckerman, M. E.; Chandra, A.; Marx, D. A statistical mechanical theory of proton transport kinetics in hydrogen-bonded networks based on population correlation functions with applications to acids and bases. *J. Chem. Phys.* **2010**, *133*, 124108.
(41) Siepmann, J. I.; Sprik, M. Influence of surface topology and electrostatic potential on water/electrode systems. *J. Chem. Phys.* **1995**, *102*, 511−524.
(42) Limmer, D. T.; Merlet, C.; Salanne, M.; Chandler, D.; Madden, P. A.; Roij, R.; Rotenberg, B. Charge Fluctuations in Nanoscale Capacitors. *Phys. Rev. Lett.* **2013**, *111*, 106102.
(43) Merlet, C.; Péan, C.; Rotenberg, B.; Madden, P. A.; Simon, P.; Salanne, M. Simulating Supercapacitors: Can We Model Electrodes As Constant Charge Surfaces? *J. Phys. Chem. Lett.* **2013**, *4*, 264−268.
(44) Petersen, M. K.; Kumar, R.; White, H. S.; Voth, G. A. A Computationally Efficient Treatment of Polarizable Electrochemical Cells Held at a Constant Potential. *J. Phys. Chem. C* **2012**, *116*, 4903−4912.
(45) http://www.chem.utah.edu/directory/faculty/white.html.
(46) Lange, A. W.; Voth, G. A. Multi-State Approach to Chemical Reactivity in Fragment Based Quantum Chemistry Calculations. *J. Chem. Theory Comput.* **2013**, *9*, 4018−4025.
(47) Griffiths, D. *Introduction to Electrodynamics*, 3rd ed.; Prentice Hall: Upper Saddle River, NJ, 1998.
(48) Frisch, M. J.; Trucks, G. W.; Schlegel, H. B.; Scuseria, G. E.; Robb, M. A.; Cheeseman, J. R.; Scalmani, G.; Barone, V.; Mennucci, B.; Petersson, G. A.; Nakatsuji, H.; Caricato, M.; Li, X.; Hratchian, H. P.; Izmaylov, A. F.; Bloino, J.; Zheng, G.; Sonnenberg, J. L.; Hada, M.; Ehara, M.; Toyota, K.; Fukuda, R.; Hasegawa, J.; Ishida, M.; Nakajima, T.; Honda, Y.; Kitao, O.; Nakai, H.; Vreven, T.; Montgomery, J. A., Jr.; Peralta, J. E.; Ogliaro, F.; Bearpark, M.; Heyd, J. J.; Brothers, E.; Kudin, K. N.; Staroverov, V. N.; Kobayashi, R.; Normand, J.; Raghavachari, K.; Rendell, A.; Burant, J. C.; Iyengar, S. S.; Tomasi, J.; Cossi, M.; Rega, N.; Millam, N. J.; Klene, M.; Knox, J. E.; Cross, J. B.; Bakken, V.; Adamo, C.; Jaramillo, J.; Gomperts, R.; Stratmann, R. E.; Yazyev, O.; Austin, A. J.; Cammi, R.; Pomelli, C.; Ochterski, J. W.; Martin, R. L.; Morokuma, K.; Zakrzewski, V. G.; Voth, G. A.; Salvador, P.; Dannenberg, J. J.; Dapprich, S.; Daniels, A. D.; Farkas, Ö.; Foresman, J. B.; Ortiz, J. V.; Cioslowski, J.; Fox, D. J. *Gaussian 09*; Gaussian, Inc.: Wallingford, CT, 2009.
(49) Lee, C.; Yang, W.; Parr, R. Development of the Colle-Salvetti correlation-energy formula into a functional of the electron density. *Phys. Rev. B* **1988**, *37*, 785−789.
(50) Hay, P. J.; Wadt, W. R. Ab initio effective core potentials for molecular calculations. Potentials for the transition metal atoms Sc to Hg. *J. Chem. Phys.* **1985**, *82*, 270−283.
(51) Krishnan, R.; Binkley, J. S.; Seeger, R.; Pople, J. A. Self-consistent molecular orbital methods. XX. A basis set for correlated wave functions. *J. Chem. Phys.* **1980**, *72*, 650−654.
(52) Wu, Y.; Tepper, H. L.; Voth, G. A. Flexible simple point-charge water model with improved liquid-state properties. *J. Chem. Phys.* **2006**, *124*, 024503.
(53) MacKerell, J. A. D.; Bashford, D.; Dunbrack, J. R. L.; Evanseck, J. D.; Field, M. J.; Fischer, S.; Gao, J.; Guo, H.; Ha, S.; Joseph-McCarthy, D.; Kuchnir, L.; Kuczera, K.; Lau, F. T. K.; Mattos, C.; Michnick, S.; Ngo, T.; Nguyen, D. T.; Prodhom, B.; Reiher, W. E.; Roux, B.; Schlenkrich, M.; Smith, J. C.; Stote, R.; Straub, J.; Watanabe, M.; Wiórkiewicz-Kuczera, J.; Yin, D.; Karplus, M. All-Atom Empirical Potential for Molecular Modeling and Dynamics Studies of Proteins. *J. Phys. Chem. B* **1998**, *102*, 3586−3616.
(54) Plimpton, S. Fast Parallel Algorithms for Short-Range Molecular Dynamics. *J. Comput. Phys.* **1995**, *117*, 1−19.
(55) Berendsen, H. J. C.; Postma, J. P. M.; van Gunsteren, W. F.; DiNola, A.; Haak, J. R. Molecular dynamics with coupling to an external bath. *J. Chem. Phys.* **1984**, *81*, 3684−3690.
(56) Hockney, R. W.; Eastwood, J. W. *Computer Simulation Using Particles*; Adam Hilger: Philadelphia, PA, 1988.
(57) Yeh, I.; Berkowitz, M. L. Ewald summation for systems with slab geometry. *J. Chem. Phys.* **1999**, *111*, 3155−3162.
(58) Errington, J. R.; Debenedetti, P. G. Relationship between structural order and the anomalies of liquid water. *Nature* **2001**, *409*, 318−321.
(59) Kumar, P.; Buldyrev, S. V.; Stanley, H. E. A tetrahedral entropy for water. *Proc. Natl. Acad. Sci. U.S.A.* **2009**, *106*, 22130−22134.
(60) Petersen, M. K.; Voth, G. A. Characterization of the Solvation and Transport of the Hydrated Proton in the Perfluorosulfonic Acid Membrane Nafion. *J. Phys. Chem. B* **2006**, *110*, 18594−18600.
(61) Xu, J.; Izvekov, S.; Voth, G. A. Structure and Dynamics of Concentrated Hydrochloric Acid Solutions. *J. Phys. Chem. B* **2010**, *114*, 9555−9562.
(62) Tse, Y. S.; Herring, A. M.; Kim, K.; Voth, G. A. Molecular Dynamics Simulations of Proton Transport in 3M and Nafion Perfluorosulfonic Acid Membranes. *J. Phys. Chem. C* **2013**, *117*, 8079−8091.
(63) Chen, H.; Yan, T.; Voth, G. A. A Computer Simulation Model for Proton Transport in Liquid Imidazole. *J. Phys. Chem. A* **2009**, *113*, 4507−4517.
(64) White, R. J.; White, H. S. Electrochemistry in Nanometer-Wide Electrochemical Cells. *Langmuir* **2008**, *24*, 2850−2855.